

Evolution of the star formation histories of BLAST galaxies

Simon Dye^{1*}, Steve Eales¹, Lorenzo Moncelsi¹, Enzo Pascale¹

¹Cardiff University, School of Physics & Astronomy, Queens Buildings, The Parade, Cardiff, CF24 3AA, U.K.

Document in prep.

ABSTRACT

We have measured star formation histories (SFHs) and stellar masses of galaxies detected by the Balloon-borne Large Aperture Sub-millimetre Telescope (BLAST) over $\sim 9 \text{ deg}^2$ centred on the Chandra Deep Field South. We have applied the recently developed SFH reconstruction method of Dye et al. to optical, near-infrared and mid-infrared photometry of 92 BLAST galaxies. We find significant differences between the SFHs of low mass ($\lesssim 10^{11} M_{\odot}$) and high mass ($\gtrsim 10^{11} M_{\odot}$) systems. On average, low mass systems exhibit a dominant late burst of star formation which creates a large fraction of their stellar mass. Conversely, high mass systems tend to have a significant amount of stellar mass that formed much earlier. We also find that the high mass SFHs evolve more strongly than the low mass SFHs. These findings are consistent with the phenomenon of downsizing observed in optically selected samples of galaxies.

Key words: galaxies: star formation – submillimetre: galaxies – galaxies: evolution

1 INTRODUCTION

Encoded in every galaxy’s spectrum is a record of its entire life from birth, up to the epoch at which it is observed. Unlocking this information, by determining the variation in star formation rate (SFR) with age, is a key step towards understanding how galaxies form and evolve. The measurement of star formation histories (SFHs) therefore plays a crucial role in the development of an accurate model to describe the range of processes experienced by galaxies and the subsequent formation of stellar mass in the Universe.

Currently, the most elusive population of galaxies are systems heavily obscured by dust, often detected only at sub-millimetre (submm) wavelengths. Approximately half of all light emitted by galaxies is absorbed by dust and re-radiated in the submm. However, compared with studies at optical wavelengths, little is known about submm galaxies, in particular, how they relate to local systems. Submm selected samples of galaxies therefore provide an unavoidably important set of constraints on a complete and self-consistent view of galaxy formation mechanisms.

(Dye et al. 2008) conducted an analysis of the SFHs of $850 \mu\text{m}$ selected galaxies and found that these systems are typically dominated by a strong burst of star formation late in their history, but that around half of their stellar population had already formed over the first half of their lives. This study also revealed a surprising deficit of high mass ($> 5 \times 10^{11} M_{\odot}$) systems at redshifts $z < 2$, strong

evidence of downsizing in the population, possibly explained by the evolution of these systems into massive ellipticals.

The Balloon-borne Large Aperture Sub-millimetre Telescope (BLAST) recently provided a catalogue of hundreds of submm selected galaxies over $\sim 9 \text{ deg}^2$ of sky (Devlin et al. 2009) centred on the Chandra Deep Field South (CDFS). The identification of radio and $24 \mu\text{m}$ counterparts to the majority of sources (Dye et al. 2009) combined with follow-up optical spectroscopy (Eales et al. 2009) and a comprehensive suite of archival optical, near-infrared (near-IR) and mid-infrared (mid-IR) imaging results in these data being the largest, most thoroughly characterised and carefully processed sample of $250\text{--}500 \mu\text{m}$ selected sources to date. The sample and its supporting multi-wavelength data therefore presents a perfect opportunity to conduct a study of SFHs of submm selected galaxies.

The purpose of this letter is therefore to carry out an investigation of the SFHs and stellar masses of BLAST galaxies in a similar vein to the study of $850 \mu\text{m}$ selected galaxies conducted by Dye et al. (2008). To compute SFHs, we have used the recently developed method of Dye (2008). We have applied the method to optical, near-IR and mid-IR photometry of the counterparts to the BLAST sources identified by Dye et al. (2009).

In Section 2 we briefly outline the procedure used for applying the SFH reconstruction method. Section 3 describes the data. The results are presented in Section 4. Finally, we summarise in Section 5. Throughout this letter, the following cosmological parameters are assumed; $H_0 = 71 \text{ km s}^{-1} \text{ Mpc}^{-1}$, $\Omega_m = 0.27$, $\Omega_{\Lambda} = 0.73$.

* E-mail: s.dye@astro.cf.ac.uk

2 SFH RECONSTRUCTION METHOD

Dye (2008) provides a detailed description of the SFH reconstruction method. The purpose of the brief outline presented here is both for completeness and to give specific details of the procedure we have used in this implementation.

2.1 Method Outline

The method divides a galaxy's history into discrete blocks of time. This results in a relatively low resolution SFH, but one that does not adhere to a prescribed (i.e., potentially biased) parametric form. Using a synthetic library of simple stellar population (SSP) SEDs, the fluxes resulting from a constant SFR normalised to one solar mass in each block, as measured in the observer frame across a range of filters, are calculated. Finding the contribution of flux from each block in each filter that best fits a set of observed fluxes is a linear problem that can be solved exactly. The solution directly yields the galaxy's SFH and stellar mass. In this letter, we have used the stellar SED libraries of Maraston (2005) and, for comparison, Bruzual & Charlot (2003).

Starting with a SSP SED, L_λ^{SSP} , of metallicity Z , a composite stellar population (CSP) SED, L_λ^i , is generated for the i th block of constant star formation in a given galaxy using

$$L_\lambda^i = \frac{1}{\Delta t_i} \int_{t_{i-1}}^{t_i} dt' L_\lambda^{\text{SSP}}(\tau(z) - t') \quad (1)$$

where the block spans the period t_{i-1} to t_i in the galaxy's history and τ is the age of the galaxy (i.e., the age of the Universe today minus the look-back time to the galaxy). The quantity $\Delta t_i = t_i - t_{i-1}$ ensures that the CSP is normalised to one solar mass. The above integral is evaluated by interpolating linearly in $\log(t)$ between the discrete time intervals at which the SSP SEDs are given in the libraries. Note that the method assumes that Z does not vary with age.

To model the effects of extinction on the final SED (i.e., the SED from all blocks in the SFH), reddening is applied. This is achieved by individually reddening the CSP of each block using $L_{\lambda,R}^i = L_\lambda^i 10^{-0.4k(\lambda)A_V/R_V}$ where, A_V is the extinction, $R_V = 4.05$ and the Calzetti Law (Calzetti et al. 2000) is used for $k(\lambda)$. The model flux (i.e., photon count) observed in filter j from a given block i in the SFH when the galaxy lies at a redshift z is then

$$F_{ij} = \frac{1}{4\pi d_L^2} \int d\lambda \frac{\lambda L_{\lambda,R}^i(\lambda/(1+z))T_j(\lambda)}{(1+z)hc} \quad (2)$$

where d_L is the luminosity distance and T_j is the transmission curve of filter j .

To find the normalisations a_i which result in a set of model fluxes that best fits the observed fluxes, the following χ^2 function is minimised

$$\chi^2 = \sum_j \frac{(\sum_i^{N_{\text{block}}} a_i F_{ij} - F_j^{\text{obs}})^2}{\sigma_j^2} \quad (3)$$

where F_j^{obs} is the galaxy flux observed in filter j and σ_j is its error. The sum in i acts over all N_{block} SFH blocks. The minimum χ^2 occurs when the condition $\partial\chi^2/\partial a_i =$

0 is simultaneously satisfied for all a_i . This gives a set of equations linear in the a_i which are solvable using a standard matrix inversion (see Dye 2008, for more details). The a_i are the stellar masses formed in each block so that the total stellar mass of the galaxy is the sum $M_* = \sum_i^{N_{\text{block}}} a_i$. The SFRs and hence the SFH is then given directly by dividing the a_i by the time spanned by each corresponding block. Formal errors on the a_i are obtained from the covariance matrix, computed in a simple additional step. To allow for uncertainty in source redshift, we performed a Monte Carlo simulation, randomising the redshift according to its error, and combined the resulting scatter in the a_i in quadrature with the formal errors. The total error on the stellar mass was obtained in the same manner.

As discussed in Dye (2008), regularisation must be applied to ensure that the linear solution is well defined. The strength of regularisation is controlled by a parameter referred to as the regularisation weight, denoted w hereafter.

2.2 Fitting Procedure

The procedure outlined in the previous section is a single linear step which computes the SFH that gives the best fit (i.e., minimum χ^2) to an observed set of fluxes for a given set of parameters z , Z , A_V , N_{block} and w . This step is nested inside a non-linear search for the set of parameter values that gives the best overall fit to the observed fluxes. As discussed in Dye (2008), finding the best global solution can not be achieved by minimising χ^2 because the effective number of degrees of freedom depends on w in an unquantifiable manner. It is therefore not possible to use χ^2 to make a fair comparison of the goodness-of-fit between two parameter sets with differing values of w . To make a fair comparison, one must turn to Bayesian statistics and treat regularisation as a prior. In this way, the Bayesian evidence, denoted ϵ hereafter, allows different sets of parameters to be ranked fairly. The best global solution is that which maximises ϵ .

We investigated a range of different schemes to maximise ϵ . The most efficient and reliable scheme that we found combines a standard grid search with a downhill simplex minimisation to find the minimum of $-\ln \epsilon$ (hence the maximum of ϵ). We use the simplex routine, linearly computing the SFH and evaluating ϵ each time, to find the best pair of values of A_V and $\log w$ whilst keeping Z and N_{block} fixed. Then, at the outer-most level, we step through a grid of regularly spaced trial values of $\log Z$ and N_{block} over the ranges $-2 < \log_{10}(Z/Z_\odot) < 0.3$ and $2 < N_{\text{block}} < 5$. The value of z was fixed at the measured redshift of the galaxy (see Section 3) at all times.

3 DATA

Dye et al. (2009) found optical counterparts to 114 of the ~ 130 radio- and/or $24 \mu\text{m}$ -identified BLAST sources located in the region covered by their optical data. All 114 sources were detected at $\geq 5\sigma$ in at least one of the three BLAST bands (250, 350 and $500 \mu\text{m}$). As described below, we acquired a range of optical, near-IR and mid-IR photometry for these 114 sources. We rejected 12 sources on the basis of having less than five photometric data points,

applying our analysis to the remaining 102. In all cases, we used total magnitudes/fluxes.

Optical photometry was taken from either the Spitzer Wide-area InfraRed Extragalactic survey (SWIRE; Lonsdale et al. 2004), or the 17 band COMBO-17 (Classifying Objects by Medium-Band Observations in 17 filters) survey (Wolf et al. 2004). The SWIRE survey covers $\sim 5 \text{ deg}^2$ to a depth of $r \simeq 24.5$ (Vega, 5σ) and COMBO-17 covers $\sim 0.25 \text{ deg}^2$ to $R \simeq 26.0$ (Vega, 5σ). The SWIRE optical catalogue directly provides total magnitudes. For COMBO-17, we computed total magnitudes from aperture fluxes in all filters using the given source-specific correction derived in the R band. For objects detected in both surveys, we amalgamated both sets of photometry.

For the near-IR, we used the J and K photometry from the Multi-wavelength Survey by Yale-Chile (MUSYC Gawiser et al. 2006). This reaches depths of 22.1 and 20.5 (Vega, 5σ) in J and K respectively. Although MUSYC only covers $\sim 0.3 \text{ deg}^2$, the survey area is centred on the CDFS where the deep BLAST observations were made (see Dye et al. 2009), hence we obtained near-IR photometry for 52 of the 102 sources. The MUSYC catalogue gives aperture and total K band fluxes. We obtained total J band fluxes by scaling the aperture fluxes by the total:aperture K band flux ratio.

Mid-IR photometry was taken from the SWIRE survey which completely encompasses the region containing the BLAST sources considered in the present work. We used 3.6 and $4.5 \mu\text{m}$ fluxes which are limited to a 10σ sensitivity of $10 \mu\text{Jy}$ at $3.6 \mu\text{m}$ and a 5σ sensitivity of $10 \mu\text{Jy}$ at $4.5 \mu\text{m}$. For reconstructing source SFHs, we only used $3.6 \mu\text{m}$ photometry for objects with redshifts $z > 0.6$ and additionally $4.5 \mu\text{m}$ photometry only for objects at $z > 1$. These redshift limits ensure that the observed photometry does not extend beyond the restframe K band where the empirical stellar component of the Maraston SEDs ends.

We imposed a minimum photometric error of 0.05 mag for all photometry to allow for zero point uncertainties and mismatches in calibration between different datasets.

In terms of redshifts, 47 of the sources have spectroscopic redshifts taken from Monceli et al. (2010). For the remainder, we used the photometric redshifts assigned in Dye et al. (2009). These are taken from either Rowan-Robinson et al. (2008) which uses the SWIRE optical photometry as well as the SWIRE 3.6 and $4.5 \mu\text{m}$ data or from COMBO-17.

4 RESULTS

We applied the procedure outlined in Section 2.2 to maximise the Bayesian evidence for each galaxy. We found that 5-10% of reconstructions resulted in very poor fits to the observed photometry and/or gave unphysical SFHs (i.e., strongly negative bursts of star formation). These failures were readily discarded by applying a cut in the evidence of $\ln \epsilon > -100$. This removed 10 of the 102 sources, including three low redshift galaxies ($z < 0.1$) which are optically well resolved (up to $\sim 50''$ in diameter) and therefore susceptible to strong photometric biases between the different catalogues. All analysis that follows in this letter is applied to the remaining 92 systems.

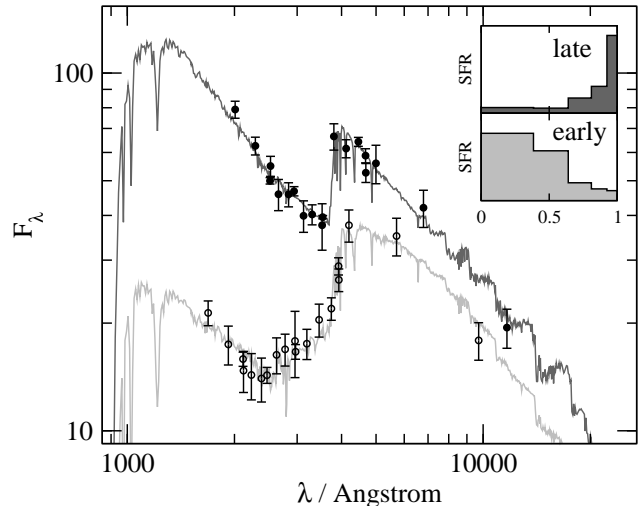


Figure 1. Example rest-frame SEDs fitted to optical and near-IR photometry of two BLAST sources. The darker SED, corresponding to a $z \simeq 0.8$ galaxy with observed photometry plotted as filled photometric data points, is fit with an SFH where 60% of its stellar mass was formed in the last 10% of its history and 15% formed in the first half. The lighter SED, corresponding to a $z \simeq 1.2$ galaxy with observed photometry plotted as unfilled data points, has a SFH with only 3% of its stellar mass formed in the last 10% of its history and 85% formed in the first half. Fluxes are in arbitrary units and SEDs are independently scaled for clarity. Inset panels show the SFR versus fractional galaxy age from birth ($t = 0$) to the epoch its observed ($t = 1$) for each SED.

Our findings indicate that the vast majority of BLAST galaxies have SFHs which peak at late times. Around 10% of systems are more consistent with early type SEDs having formed at least three quarters of their stellar mass in the first half of their lives and less than 2% of their mass in the last tenth of their lives. Figure 1 shows two fairly extreme example SEDs of BLAST sources, one dominated by late star formation and the other having formed nearly all of its stars early on, to illustrate the range SEDs observed.

Figure 2 shows how the stellar masses vary with redshift. There is an obvious trend of increasing mass with increasing redshift, limited by the rarity of high mass galaxies at one end of the scale and the sensitivity to low luminosity at the other. The few low mass outliers are systems dominated by extremely late and intense bursts of star formation and hence have low mass-to-light ratios. Four of the 92 objects are flagged as having a dominant active galactic nuclear component by Monceli et al. (2010) based on their spectral line strength ratio $[\text{NII}]\lambda 658.3/\text{H}\alpha$. These four objects are all located near the high mass edge of the envelope shown in Figure 2 and spread throughout the redshift range.

We investigated the possibility of evolution in the SFHs and whether this depends on mass by segregating the sample of 92 galaxies into four approximately equally sized sub-samples divided at $z = 0.5$ and $M_* = 9 \times 10^{10} M_\odot$. Figure 3 shows the average SFH for each sub-sample, rebinned to a common resolution of five blocks. In the averaging, we normalised the SFH of each galaxy to units of fractional total stellar mass formed per fractional age so that the integral of SFH over fractional age (i.e., the total stellar mass) is equal to unity.

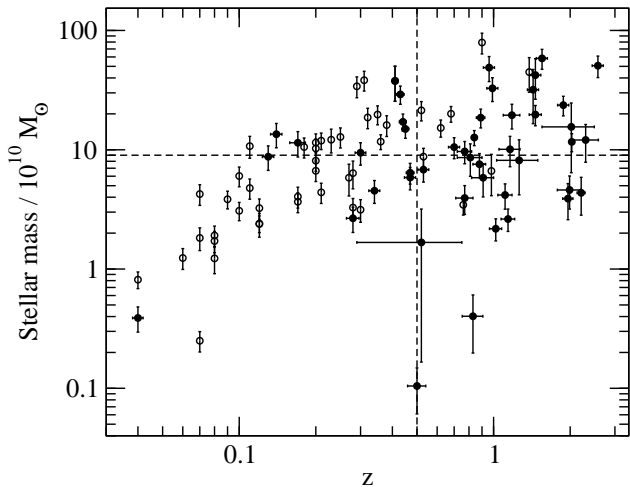


Figure 2. Stellar mass in units $10^{10} M_{\odot}$ versus redshift for the BLAST sources. The dashed lines at $z = 0.5$ and $9 \times 10^{10} M_{\odot}$ divide the sample into four approximately equal sub-samples which we have then used in our analysis of SFH evolution by mass. Open points indicate sources where a spectroscopic redshift has been used and filled points with errors show the remaining sources with photometric redshifts. Mass errors include photometric and redshift uncertainties.

The most striking feature seen in the plots is the difference between the low and high mass sub-samples. On average, both low mass SFHs are dominated by a late burst of strong star formation activity accounting for $\sim 40\%$ of the total stellar mass. Conversely, both high mass SFHs show that a much smaller fraction of stellar mass ($\sim 5 - 10\%$) is created during this last period, the majority of mass being formed at earlier times.

Another obvious effect seen in Figure 3 is that the high mass sources exhibit a more prominent difference in their SFHs in moving from high to low redshifts than the low mass sources. The high mass sources have therefore, by this definition, undergone more evolution. To quantify the significance of this, we computed the reduced χ^2 statistic between the low and high redshift SFHs for the low and high mass sub-samples in turn. For the high mass SFHs, the statistic is $\chi_r^2 = 3.57 \pm 0.63$ compared to $\chi_r^2 = 0.51 \pm 0.63$ for the low mass SFHs. The change at high mass is therefore significant at the $\sim 3\sigma$ level whereas the low mass source SFHs are consistent with no change. This is synonymous with down-sizing where the instantaneous star formation rate in high mass galaxies evolves more strongly than that in low mass systems (e.g., Heavens et al. 2004).

The SFHs computed in terms of fractional mass and fractional galaxy age are a very useful diagnostic since they effectively normalise out the large scatter in mass and redshift present in the necessarily coarsely binned sub-samples. This makes the mean trends more conspicuous. However, to compare with more traditional studies of the evolution of star formation, we estimated instantaneous absolute SFRs. For each source, we computed a ‘pseudo-instantaneous’ SFR by dividing the absolute stellar mass created in the last SFH block by the real time spanned by the block. We found that the pseudo-instantaneous SFR for the high mass sources changed from $75 \pm 26 M_{\odot} \text{ yr}^{-1}$ at high redshifts to $20 \pm 5 M_{\odot} \text{ yr}^{-1}$ at low redshifts. In comparison, the change

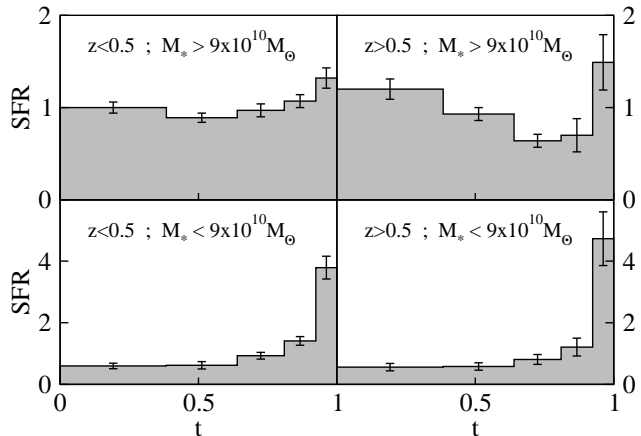


Figure 3. Mean SFHs of the four sub-samples of BLAST galaxies as delineated by the redshift and stellar mass limits indicated (see Figure 2). The error bars on each histogram bin indicate the 1σ error on the mean which includes the formal error from the linear inversion and the uncertainty in source redshift computed in the Monte Carlo analysis (see Section 2.1). All SFRs are expressed in units of fraction of total stellar mass per fractional age (i.e., the area under each histogram in these units is 1). The fractional age varies from $t = 0$ at $z = \infty$ to $t = 1$ at the epoch of the galaxy’s redshift.

for the low mass sources is from from $43 \pm 23 M_{\odot} \text{ yr}^{-1}$ at high redshifts to $9 \pm 2 M_{\odot} \text{ yr}^{-1}$ at low redshifts. The conclusion is therefore that we detect no significant difference in the evolution of the pseudo-instantaneous SFR between the high and low mass sources. To detect an absolute trend such as this, more sources would be required to enable finer binning in mass and redshift.

An interesting point to note is that the rate of formation of stellar mass, which is highest at early and at late times in the high mass, high redshift sub-sample, is very similar to that measured by Dye et al. (2008) for $850 \mu\text{m}$ selected sources. This is perhaps not too surprising given the large overlap of this sub-sample with the $850 \mu\text{m}$ sample which has a median value of redshift and $\log_{10}(M/M_{\odot})$ of 1.6 ± 1.0 and 11.5 ± 0.5 respectively, where the errors give the standard deviation. The fact that such a large stellar population was already in place at higher redshifts suggests that the peak star formation rate occurred significantly earlier in the history of the Universe for high mass systems than for low mass systems. This behaviour was observed by Heavens et al. (2004) for optically selected galaxies.

To verify the robustness of our results, we conducted a series of tests. The first was to see if the inferred SFHs are intrinsic or merely the effect of reddening. For example, an intrinsically late-type galaxy with strong reddening could give rise to a reconstructed SFH with artificially suppressed late star formation. We therefore plotted the fraction of mass formed in the last 10% of each galaxy’s history, $M_{10\%}$, against A_V . Since late activity strongly dominates the shape of the observed SED, $M_{10\%}$ is a sensitive indicator of SED type. Therefore, a strong degeneracy between the inferred lateness of an SED and extinction would manifest itself as an obvious positive correlation between $M_{10\%}$ and A_V (if the SED is more reddened, more late stellar mass is required to maintain a fit to the observed photometry). Figure 4 shows these two quantities plotted for all galaxies

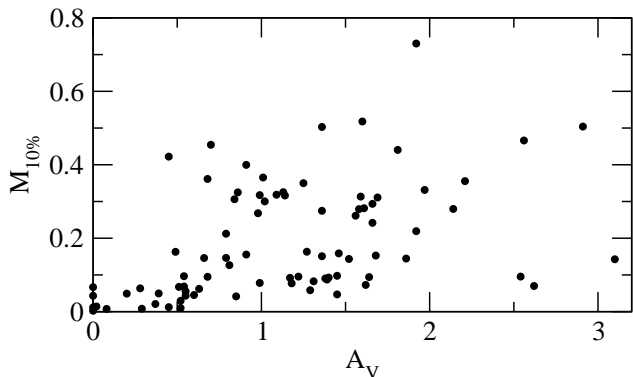


Figure 4. The relationship between the fraction of mass formed in the last 10% of each galaxy's history, $M_{10\%}$, and A_V .

in our sample. The scatter is large, although there is some evidence of a correlation. For example, all galaxies which form less than 10% of mass in the last 10% of their history have values of $A_V < 0.5$. However, this is at least partly explained by the simple fact that elliptical galaxies tend to have little or no dust. We therefore conclude that any degeneracies between reddening and reconstructed SFHs do not significantly affect the results described in this letter.

The second test addresses the concern that there may be a potential bias introduced by including the mid-IR photometry based on redshift. We therefore isolated all sources whose SED fitting used mid-IR photometry and repeated the fitting without it. Within the errors, which were made larger by the lack of mid-IR photometry, we found negligible differences in the results.

As a third test, we repeated the analysis using the stellar SED library of (Bruzual & Charlot 2003). The only significant difference we found was that the stellar masses were an average of 40% higher than those computed with the Maraston SEDs. The reconstructed SFHs of the high mass sources also showed slightly higher fractions of mass at early times, but this was within the errors.

Our final test was to repeat the analysis without the four sources flagged as having strong AGN activity. The differences were again negligible.

5 SUMMARY

Using optical, near-IR and mid-IR photometry, we have reconstructed the SFHs of a sample of 92 submm sources detected by BLAST. Their SFRs peak at late times on average, consistent with the high instantaneous SFR inferred from their submm emission. We divided the sample by mass and redshift into four sub-samples. Our findings clearly indicate that the low mass sources form a much higher fraction of their stellar mass at late times than the high mass sources, consistent with the notion that the SFRs of higher mass galaxies peaked at earlier times. Furthermore, the SFHs of the higher mass sources evolve more strongly than the SFHs of lower mass sources. This behaviour is synonymous with downsizing observed in optically-selected samples of galaxies. Finally, our high mass, high redshift sub-sample shows evidence of stellar mass being formed predominantly at late and at early times, but less so when the galaxies are middle-

aged. The same trend was also observed in the sample of $850\mu\text{m}$ selected sources by Dye et al. (2008), although this is perhaps not surprising given the similar range of masses and redshifts in the sub-sample.

This letter has analysed the optical counterparts to approximately one third of the full BLAST detected sample of galaxies presented in Dye et al. (2009). It is now understood that a significant fraction of the galaxies detected solely at $500\mu\text{m}$, are the result of flux boosting and therefore probably not real (see Moncelsi et al. 2010). Our sample of 92 galaxies contains five $500\mu\text{m}$ -only detections. Based on the findings of Moncelsi et al., we expect that only ~ 1 of these is not real. Of the BLAST sources believed to be real, around 50% of these were not identified with radio and/or $24\mu\text{m}$ counterparts. Whilst some of these may have been detected in the optical/near-IR surveys used in this letter, it is likely that the majority will be heavily dust obscured systems lying at higher redshifts (see Dye et al. 2009).

Although we have allowed for extinction by dust, there could be regions in the BLAST galaxies completely obscured at rest-frame optical/near-IR wavelengths. Dye et al. (2008) made a correction for this effect using far-IR/submm bolometric luminosity, finding that fully obscured star formation could result in the generation of up to an additional 50% of the galaxy's total stellar mass. It is likely that this fraction is even larger for those BLAST galaxies with radio/ $24\mu\text{m}$ counterparts but no optical/IR counterparts.

The findings described in this letter represent a taster of what would be possible with a significantly larger sample of sources. Although the BLAST data currently offer the largest and most thoroughly processed sample of galaxies selected over the wavelength range of 200 to $600\mu\text{m}$ to date, the increased sensitivity and resolution of the Herschel space observatory, which recently started operation, will soon provide vastly increased numbers of sources. This will enable significantly reduced uncertainties and therefore much improved constraints on models of galaxy evolution and formation. Nevertheless, the BLAST data will still provide a very valuable benchmark for the Herschel data and the various analyses that will emerge for some time to come.

Acknowledgements

SD is supported by the UK Science and Technology Facilities Council.

REFERENCES

- Bruzual, G. & Charlot, S., 2003, MNRAS, 344, 1000
- Calzetti, D., Armus, L., Bohlin, R. C., Kinney, A. L., Koorneef J., Storchi-Bermann, T., 2000, ApJ, 533, 682
- Devlin, M. J., et al., 2009, Nature, 458, 737
- Dye, S., 2008, MNRAS, 389, 1293
- Dye, S., et al., 2008, MNRAS, 386, 1107
- Dye, S., et al., 2009, ApJ, 703, 285
- Eales, S. A., et al., 2009, ApJ, 707, 1779
- Gawiser, E., et al., 2006, ApJS, 162, 1
- Heavens, A. F., Panter, B., Jimenez, R., Dunlop, J. S., 2004, Nature, 428, 625
- Lonsdale, C. J., et al., 2004, ApJS, 154, 54
- Maraston, C., 2005, MNRAS, 362., 799

Moncelsi, L., et al., 2010, ApJ, submitted
Rowan-Robinson, M., et al., 2008, 386, 697
Wolf, C., et al., 2004, A&A, 421, 913